Product Analysis and Thermodynamic Simulations from the Pyrolysis of Several Biomass Feedstocks

Jieling Zhang,[†] Hossein Toghiani,*[,†] Dinesh Mohan,*[,‡,§] Charles U. Pittman, Jr.,[‡] and Rebecca K. Toghiani[†]

Dave C. Swalm School of Chemical Engineering, Mississippi State University, Mississippi State, Mississippi 39762, Department of Chemistry, Mississippi State University, Post Office Box 9573, Mississippi State, Mississippi 39762, and Environmental Chemistry Division, Industrial Toxicology Research Centre, Post Office Box 80, Mahatma Gandhi Marg, Lucknow 226001, India

Received December 28, 2006. Revised Manuscript Received March 21, 2007

The pyrolysis of southern pine, red oak, and sweet gum sawdust is reported. Pyrolysis experiments were conducted under either a helium or nitrogen atmosphere at ∼371−871 °C, to determine the balance between liquid and gas products. Gas- and liquid-phase pyrolysis products were identified using gas chromatography (GC) and GC/mass spectrometry (MS). A total of 109 liquid and 40 gas compounds were identified. A total of 59 chemical compounds (35 liquids and 24 gaseous products) were quantitatively determined. The influence of the gas-phase residence time and biomass feed particle size were studied. The gas residence time determined the extent of secondary reactions. Very short residence times enhanced liquid production versus gas production. Particle sizes ($d < 105$ μm, 105 μm $< d <$ 149 μm, 149 μm $< d <$ 297 μm, and $d > 297$ μm) did not have a pronounced effect on either the yield or product distributions, indicating that heat-transfer limitations within the particles were negligible. The pyrolysis of pine, red oak, and sweet gum sawdust yielded similar product distributions. Simulations were conducted using the ASPEN/SP software package based on Gibbs energy minimization. At high temperatures, dominant species were hydrogen and carbon monoxide, while at lower temperatures, methane, carbon dioxide, and water were the predominant species. Above 871 °C, further increases in the temperature did not affect the product distribution. Lower gasification temperatures and higher steam/carbon ratios resulted in higher hydrogen and carbon monoxide production.

1. Introduction

The need for resource conservation and renewable fuels has promoted efforts to convert biomass to liquid fuels, gases, and specific chemicals since the oil crisis in the mid-1970s.[1,2] Oil is a nonrenewable resource, and the United States is heavily reliant on foreign oil sources. These are excellent incentives for developing renewable energy sources. The accelerated rate of growth of energy consumption in Asia, particularly China and India, raises this incentive for all countries. In addition, fossil fuel combustion adds carbon dioxide to the atmosphere, thought to contribute to global warning. Conversely, the use of biomass is more CO_2-neutral. Furthermore, biomass represents about 80% of energy resources in countries such as India or subtropical Africa (38% on a worldwide scale).[3] Biological and thermochemical conversions are now recognized as the most efficient ways to utilize biomass for fuels.

Biomass fast pyrolysis is a promising route to liquid fuels.[1,4−8] Pyrolysis of biomass in an inert atmosphere produces gaseous products (CO_2, H_2, CO, CH_4, C_2H_2, C_2H_4, C_6H_6, etc.), liquids (tars, high-molecular hydrocarbons, and water), and solid char. The variation of the heating rate and temperature modifies the distribution of gases, liquids, and chars obtained. Fast pyrolysis to maximize biocrude liquid yields requires very high heating rates (>100 °C/min), elimination of heat-transfer limitations through the use of finely ground biomass (<1 mm), temperatures from 425 to 500 °C, and rapid vapor/aerosol condensation.[1,5,8] Maximum pyrolysis oil yields occur from 425 to 557 °C.[5,9−12]

* To whom correspondence should be addressed. E-mail: hossein@che.msstate.edu (H.T.); dm_1967@hotmail.com (D.M.).

[†] Dave C. Swalm School of Chemical Engineering, Mississippi State University.

[‡] Department of Chemistry, Mississippi State University.

[§] Industrial Toxicology Research Centre.

(1) Mohan, D.; Pittman, C. U.; Steele, P. Pyrolysis of wood/biomass—A critical review. *Energy Fuels* **2006**, *20*, 848−889.

(2) Tsai, W. T.; Lee, M. K.; Chang, Y. M. Fast pyrolysis of rice straw, sugarcane bagasse and coconut shell in an induction-heating reactor. *J. Anal. Appl. Pyrolysis* **2006**, *76*, 230−237.

(3) Guéhenneux, G.; Baussand, P.; Brothier, M.; Poletiko, C.; Boissonnet, G. Energy production from biomass pyrolysis: A new coefficient of pyrolytic valorization. *Fuel* **2005**, *84*, 733−739.

(4) Huber, G. W.; Iborra, S.; Corma, A. Synthesis of transportation fuels from biomass: Chemistry, catalysts, and engineering. *Chem. Rev.* **2006**, *106*, 4044−4098.

(5) Bridgwater, A. V. Renewable fuels and chemicals by thermal processing of biomass. *Chem. Eng. J.* **2003**, *91*, 87−102.

(6) Bridgwater, A. V.; Czernik, S.; Piskorz, J. *An Overview of Fast Pyrolysis*; Blackwell Science: London, U.K., 2001; Vol. 2, pp 977−997.

(7) Bridgwater, A. V.; Meier, D.; Radlein, D. An overview of fast pyrolysis of biomass. *Org. Geochem.* **1999**, *30*, 1479−1493.

(8) Bridgwater, A. V.; Peacock, G. V. C. Fast pyrolysis process for biomass. *Renewable Sustainable Energy Rev.* **2000**, *4*, 1−73.

(9) Butt, D. A. E. Formation of phenols from the low-temperature fast pyrolysis of Radiata pine (*Pinus radiata*). Part 1. Influence of molecular oxygen. *J. Anal Appl. Pyrolysis* **2006**, *76*, 38−47.

(10) Piskorz, J.; Majerski, P.; Radlein, D.; Scott, D. S.; Bridgwater, A. V. Fast pyrolysis of sweet sorghum and sweet sorghum bagasse. *J. Anal. Appl. Pyrolysis* **1998**, *46*, 15−29.

(11) Murwanashyaka, J. N.; Pakdel, H.; Roy, C. Separation of syringol from birch wood-derived vacuum pyrolysis oil. *Sep. Purif. Technol.* **2001**, *24*, 155−165.

10.1021/ef0606557 CCC: $37.00 © 2007 American Chemical Society
Published on Web 05/25/2007

Wood thermal decomposition at 425−557 °C[5,9,10] in the absence of oxygen causes extensive depolymerization/fragmentation of the macromolecular structures of the wood. Primary products may further crack to yield lower molecular-weight products. Cross-linking via condensation reactions and water loss results in char formation.[13] Very high heat-transfer rates reduce char formation because volatilization is rapid, minimizing second-order polymerization rates.[14] Longer vapor residence times at pyrolysis temperatures permit more secondary vapor-phase cracking to gases, water, formic and acetic acids, and other low-molecular-weight products.[9] Therefore, rapid vapor quenching minimizes the extent of cracking.

Fast pyrolysis-derived bio-oil is used as an energy source and a feedstock for chemical production.[15−22] Methods for bio-oil include the application of ablative fluidized beds, rotating cones, vacuum moving beds, entrained flow, and transported bed reactors.[1,5−8] The physical and chemical properties of bio-oil have been discussed from various feedstocks, including wood,[11,17] bark,[18−22] agricultural wastes/residues,[23,24] nuts and seeds,[25] algae,[11,26] grasses,[11] forestry residues,[27,28] and cellulose and lignin.[29]

The compound distributions in both liquid and gaseous products are not well-known for many biomass feeds. Some studies are available on product identification and simulation.[9,30−36] Recently, Lee et al.[37] demonstrated that Sandia's perfectly stirred reactor code (PSR) is a powerful tool for the simulation of biomass pyrolysis when coupled with the Health and Safety Commission (HSC) thermodynamic software.[38]

This paper examines the pyrolysis of southern pine, red oak, and sweet gum sawdust under either helium or nitrogen as purge gases at temperatures ranging from 371 to 871 °C. The gas and liquid pyrolysis products were identified using gas chromatography (GC) and GC/mass spectrometry (MS). The influence of the gas-phase residence time and biomass feed particle size were studied. Maximizing the production of liquid products is a key objective. The gas products from the pyrolyses of biomass under inert atmospheres have much lower fuel values per unit weight than the liquid products. Also, the total heating value of liquid products, as a fraction of the entire heating value of the initial wood feed, is greater than that of converting the same weight of wood to gases. Therefore, a study of the pyrolysis products over a wide temperature range was conducted.

Pyrolyses were first simulated using ASPEN/SP process simulation software based on the assumption that chemical equilibrium was obtained. The overall objectives to undertake the present study were (1) identification and quantification of pyrolysis chemicals produced, (2) understand the influence of the reactor temperature on pyrolysis product distributions, (3) determine the influence of the gas-phase residence time on carbon monoxide, hydrogen, and methane production, (4) establish the influence of the sawdust particle size on the product distribution, and (5) study the influence of the feedstock on the product distribution.

2. Materials and Methods

All AR-grade chemicals were used. Acetone (water content of 0.17%, high purity), dichloromethane [99.9% ACS high-performance liquid chromatography (HPLC) grade], and methanol (99%) were employed. A tire pyrolysis mixture purchased from Absolute Standard, Inc. was used as the liquid product GC analysis standard, while a transformer oil gas standard from Scott Analyzed Gas and a reference gas sample from Hewlett-Packard were used as the gas product standards. The standard for permanent gases, "Airgas", was

(12) Murwanashyaka, J. N.; Pakdel, H.; Roy, C. Step-wise and one-step vacuum pyrolysis of birch-derived biomass to monitor the evolution of phenols. *J. Anal. Appl. Pyrolysis* **2001**, *60*, 219−231.

(13) Meier, D.; Faix, O. State of the art of applied fast pyrolysis of lignocellulosic materials—A review. *Bioresour. Technol.* **1999**, *68*, 71−77.

(14) Diebold, J. P.; Czernik, S. Additives to lower and stabilize the viscosity of pyrolysis oils during storage. *Energy Fuels* **1997**, *11*, 1081−1091.

(15) Huber, G. W.; Chheda, J. N.; Barrett, C. J.; Dumesic, J. A. Production of liquid alkanes by aqueous-phase processing of biomass-derived carbohydrates. *Science* **2005**, *308*, 1446−1450.

(16) Sarma, A. K.; Konwer, D. Feasibility studies for conventional refinery distillation with a (1:1) w/w of a biocrude blend with petroleum crude oil. *Energy Fuels* **2005**, *19*, 1755−1758.

(17) Kang, B.-S.; Lee, K.-H.; Park, H. J.; Park, Y.-K.; Kim, J.-S. Fast pyrolysis of radiata pine in a bench scale plant with a fluidized bed: Influence of a char separation system and reaction conditions on the production of bio-oil. *J. Anal. Appl. Pyrolysis* **2006**, *76*, 32−37.

(18) Ba, T.; Chaala, A.; Garcia-Perez, M.; Rodrigue, D.; Roy, C. Colloidal properties of bio-oils obtained by vacuum pyrolysis of softwood bark. Characterization of water-soluble and water-insoluble fractions. *Energy Fuels* **2004**, *18*, 704−712.

(19) Ba, T.; Chaala, A.; Garcia-Perez, M.; Roy, C. Colloidal properties of bio-oils obtained by vacuum pyrolysis of softwood bark. Storage stability. *Energy Fuels* **2004**, *18*, 188−201.

(20) Boucher, M. E.; Chaala, A.; Pakdel, H.; Roy, C. Bio-oils obtained by vacuum pyrolysis of softwood bark as a liquid fuel for gas turbines. Part II: Stability and ageing of bio-oil and its blends with methanol and a pyrolytic aqueous phase. *Biomass Bioenergy* **2000**, *19*, 351−361.

(21) Boucher, M. E.; Chaala, A.; Roy, C. Bio-oils obtained by vacuum pyrolysis of softwood bark as a liquid fuel for gas turbines. Part 1: Properties of bio-oil and its blends with methanol and a pyrolytic aqueous phase. *Biomass Bioenergy* **2000**, *19*, 337−350.

(22) Chaala, A.; Ba, T.; Garcia-Perez, M.; Roy, C. Colloidal properties of bio-oils obtained by vacuum pyrolysis of softwood bark: Aging and thermal stability. *Energy Fuels* **2004**, *18*, 1535−1542.

(23) Garcia-Perez, M.; Chaala, A.; Pakdel, H.; Kretschmer, D.; Rodrigue, D.; Roy, C. Multiphase structure of bio-oils. *Energy Fuels* **2006**, *20*, 364−375.

(24) Garcia-Perez, M.; Chaala, A.; Pakdel, H.; Kretschmer, D.; Rodrigue, D.; Roy, C. Evaluation of the influence of stainless steel and copper on the aging process of bio-oil. *Energy Fuels* **2006**, *20*, 786−795.

(25) Gonzalez, J. F.; Ramiro, A.; Gonzalez-Garcia, M. C.; Ganan, J.; Encinar, M. J.; Sabio, E.; Rubiales, J. Pyrolysis of almond shells. Energy applications of fractions. *Ind. Eng. Chem. Res.* **2005**, *44*, 3003−3012.

(26) Miao, X.; Wu, Q.; Yang, C. Fast pyrolysis of microalgae to produce renewable fuels. *J. Anal. Appl. Pyrolysis* **2004**, *71*, 855−863.

(27) Oasmaa, A.; Kuoppala, E.; Gust, S.; Solantausta, Y. Fast pyrolysis of forestry residue. 1. Effect of extractives on phase separation of pyrolysis liquids. *Energy Fuels* **2003**, *17*, 1−12.

(28) Oasmaa, A.; Kuoppala, E.; Solantausta, Y. Fast pyrolysis of forestry residue. 2. Physicochemical composition of product liquid. *Energy Fuels* **2003**, *17*, 433−443.

(29) Fullana, A.; Contreras, J. A.; Striebich, R. C.; Sidhu, S. S. Multidimensional GC/MS analysis of pyrolytic oils. *J. Anal. Appl. Pyrolysis* **2005**, *74*, 315−326.

(30) Duquesnoy, E.; Dinh, N. H.; Castola, V.; Casanova, J. Composition of a pyrolytic oil from *Cupressus funebris* Endl. of Vietnamese origin. *Flavour Fragrance J.* **2006**, *21*, 453−457.

(31) Yan, R.; Yang, H.; Chin, T.; Liang, D. T.; Chen, H.; Zheng, C. Influence of temperature on the distribution of gaseous products from pyrolyzing palm oil wastes. *Combust. Flame* **2005**, *142*, 24−32.

(32) Babu, B. V.; Chaurasia, A. S. Pyrolysis of biomass: Improved models for simultaneous kinetics and transport of heat, mass and momentum. *Energy Convers. Manage.* **2004**, *45*, 1297−1327.

(33) Varhegyi, G.; Antal, M. J. J.; Jakab, E.; Szabo, P. Kinetic modeling of biomass pyrolysis. *J. Anal. Appl. Pyrolysis* **1997**, *42*, 73−87.

(34) Savage, P. E. Mechanisms and kinetics models for hydrocarbon pyrolysis. *J. Anal. Appl. Pyrolysis* **2000**, *54*, 109−126.

(35) Sipilä, K.; Kuoppala, E.; Fagernäs, L.; Oasmaa, A. Characterization of biomass-based flash pyrolysis oils. *Biomass Bioenergy* **1998**, *14*, 103−113.

(36) Strezov, V.; Lucas, J. A.; Strezov, L. Experimental and modelling of the thermal regions of activity during pyrolysis of bituminous coals. *J. Anal. Appl. Pyrolysis* **2004**, *71*, 375−392.

(37) Lee, D. H.; Yang, H.; Yan, R.; Liang, D. T. Prediction of gaseous products from biomass pyrolysis through combined kinetic and thermodynamic simulations. *Fuel* **2006**, in press.

(38) Glarborg, P.; Kee, R. J.; Grcar, J. F.; Miller, J. A. *PSR: A Fortran Program for Modeling Well-Stirred Reactors*; Sandia Report, Livermore, CA, 1991.

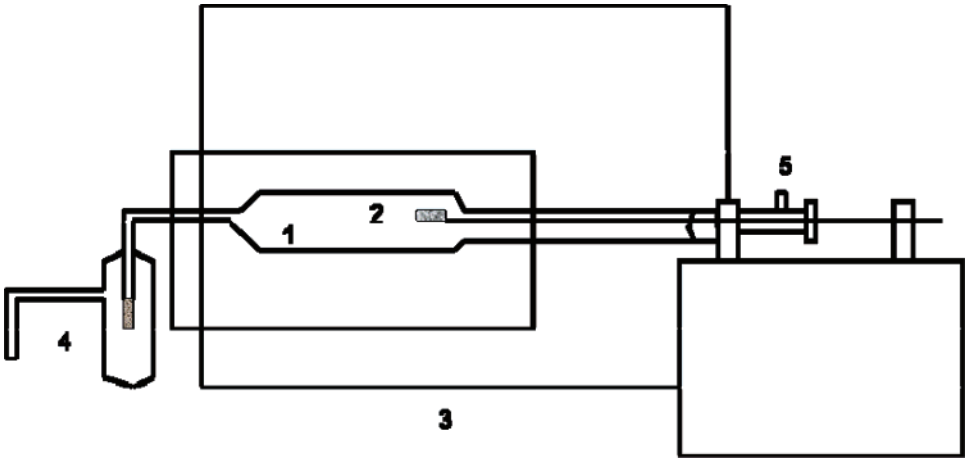

Figure 1. Pyrolysis apparatus: (1) pyrolysis tube, (2) sample boat, (3) furnace, (4) impinger, and (5) helium-purge inlet.

obtained from Gulf States. Liquid pyrolysis products were analyzed using a HP 5890 series II gas chromatograph coupled with a HP 5972 series mass selective detector (MSD). Simulation of the wood pyrolysis as well as the gasification process was performed using ASPEN/SP (Simulation Sciences, Inc.).

2.1. Pyrolysis Apparatus. Pyrolysis experiments were conducted in a modified Dohrmann DC-50/52 series total organic carbon analyzer. The horizontal fused quartz tube of the analyzer was used as a pyrolysis plug-flow reactor. The tube was divided into two zones. The sizes of the inlet and outlet zones were 180 × 10 mm (L × ID) and 120 × 20 mm (L × ID), respectively. The outlet zone further tapers to 65 × 8 mm (L × ID). The temperatures in these two zones were controlled by separate analog temperature controllers, and the temperature set points were adjusted manually. The temperatures in both zones were kept the same. The gas and liquid products were collected at the outlet of the quartz tube. The sampling time was chosen as the time interval between pushing the sample boat into the heating zone and the time the products had completely exited the reactor. This ensured that all of the products were collected.

A schematic of the experimental apparatus is shown in Figure 1. Purge gas (helium or nitrogen) was fed to the tubular reactor at the purge inlet to maintain an inlet pressure of 5 psig. Approximately 0.04 g of ground sawdust (southern pine, red oak, or sweet gum) was weighed in the platinum sample boat and then placed in the carrier plate at the end of the pushrod. The boat was positioned in the Pyrex inlet tube. The system was purged with helium or nitrogen at 20 cm^3/min for 30 min to ensure that no residual oxygen remained. The volume of the quartz tube was ~300 cm^3. The inlet and outlet zone heaters were energized to reach the operating temperature.

The outlet was connected to either a Tedlar bag for gas sampling or an impinger immersed in an ice bath for liquid sampling. Acetone, dichloromethane, and methanol were tested as condensing media to collect liquid products. The highest liquid yield was obtained with acetone as the condensing media. Therefore, acetone was used in the impinger to collect the liquid product. The pushrod was quickly moved toward the reactor so that the sample boat was placed at the center of the heating zones. Usually, this process took 1.5 s. After a designated interval, the pushrod was withdrawn, leaving the sample boat in the inlet tube to cool and be weighed. This time interval was chosen depending upon the reaction temperature. Higher reaction temperatures required shorter reaction times. Inert gas purge was maintained throughout the process.

2.2. Analytical Experimentation. A HP-1 cross-linked methyl silicon gum column (length of 50 m, diameter of 0.2 mm, and film thickness of 0.5 μm) was used for the GC analysis of liquid products. The column temperature was programmed from 45 °C (8 min hold) to 280 °C (5 min hold) at a rate of 5 °C/min. The injector and the GC/MS interface were kept at constant temperatures of 300 and 280 °C, respectively. Helium was the carrier gas, with a constant flow rate of 0.7 mL/min. Organic products were analyzed using a J&W Scientific GS-QP/N 113-3432 capillary column (length of 30 m and diameter of 0.32 mm), at a temperature programmed from 44 °C (4 min hold) to 180 °C (8 min hold) at a rate of 10 °C/min. The injector and the GC/MS interface were held constant at 200 and 280 °C, respectively. Helium (1.3 mL/min) was the carrier gas.

Noncondensable gases were analyzed using a Chrompack Carboplot P7 column (length of 25 m and diameter of 0.53 mm) and a thermal conductivity detector (TCD). The column temperature was programmed from 30 °C (3 min hold) to 80 °C (3 min hold) at a rate of 15 °C/min. Argon (7.5 mL/min) was used as the carrier gas to ensure H_2 detection.

A library MS search was performed to provide likely analyses of each component and compliment an individual analysis of each MS fragmentation pattern.

2.3. GC/MS and GC Calibration, Operation, and Quality Control. The experimental reliability of gas and liquid product yields (except for CO, H_2, and CH_4) depended upon the detection of products by the HP 5890 series II GC and the HP 5972 series MSD. Thus, MS tuning and the calibration of the GC/MS and GC were crucial for quantitative analysis.

The MSD was tuned daily using either the "Manual Tune" method followed by the "Standard Spectra Autotune" method from MS ChemStation Software or the "Standard Spectra Autotune", depending upon MSD conditions. Known amounts of the tuning standard, perfluorotributylamine (PFTBA) with major fragment ions at *m*/*e* 69, 219, and 502, were injected. The unknown samples were injected under the same conditions. One-point calibrations were used for liquid and most gas sample analyses, except for hydrogen, carbon monoxide, methane, methanol, and acetone. Response factors were determined for each compound. The calibration gas GC standard samples described above were employed. Benzene and toluene existed at high concentrations; therefore, their standards were made from pure benzene, toluene, and acetone.

Three-point calibrations were used to quantify the composition of carbon monoxide, methane, ethanol, and acetone, while two-point calibrations were used for hydrogen. Calibration plots for hydrogen, carbon monoxide, and methane gave straight lines through the origin.

Gas standards for methanol and acetone were made by injecting a known amount of liquid methanol and acetone into a Tedlar bag containing nitrogen and ensuring complete liquid evaporation.

3. Results and Discussion

3.1. Thermodynamic Simulation. Simulation of the wood pyrolysis and gasification was performed using ASPEN/SP (Simulation Sciences, Inc.) based on the assumption that chemical equilibrium was obtained. Because of the complexity

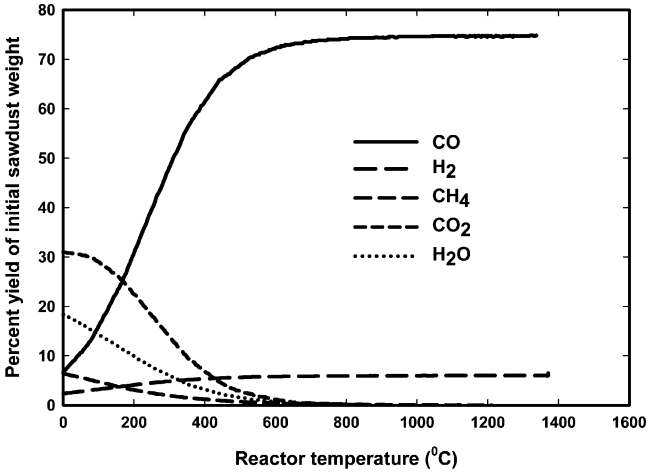

Figure 2. Effect of the reactor temperature on the predicted yields of CO, H_2, CH_4, CO_2, and H_2O from sawdust pyrolysis (from ASPEN/SP).

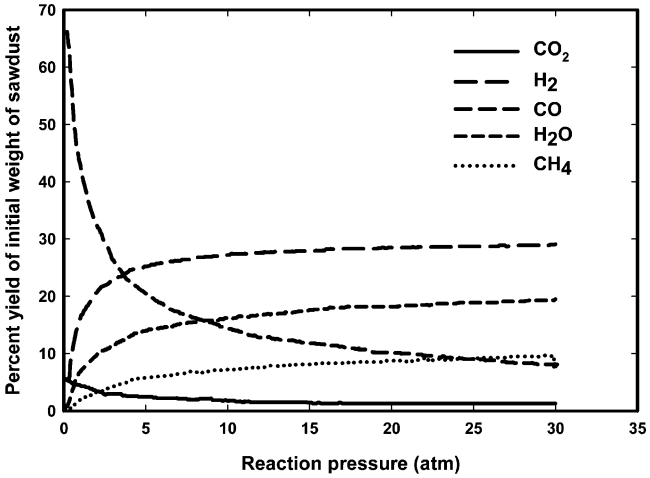

Figure 3. Effect of the reactor pressure on the predicted yields of CO, H_2, CO_2, CH_4, and H_2O at 704 °C (from ASPEN/SP).

of the reaction mechanism and the large number of reactions involved in biomass pyrolysis and gasification, the use of chemical equilibrium calculations is a convenient method to examine a product distribution and does not reflect the time dependence of the process. Chemical equilibrium calculations are based on the minimization of Gibbs energy and predict the final composition assuming that sufficient time has elapsed to achieve equilibrium. The predicted composition also reflects, to a certain extent, those species identified as present in the effluent by the modeler. In this work, the compound subset was limited to include only the following gaseous species: CO, CO_2, H_2, N_2, H_2O, and CH_4 This does significantly reduce the number of chemical reactions that are considered during the minimization process.

In fluidized bed, entrained bed, and tubular pyrolysis reactors, the residence time varies from a few seconds to a few minutes. Chemical equilibrium calculations can be compared to experiments to illustrate the extent to which equilibrium is achieved. These calculations qualitatively describe the influence of reaction conditions and predict the composition if the residence time was sufficient to achieve equilibrium.

The effects of temperature and pressure on the yield (defined as the mass of the component obtained divided by the initial mass of the sawdust sample) of CH_4, CO, H_2O, H_2, and CO_2 were predicted for different sawdust (Figures 2 and 3). The influence of the temperature and the steam/carbon mole ratio on the gasification products were also examined (Figures 4−11). The sawdust composition provided to the simulation was obtained using the ultimate and proximate analyses.[39] The ultimate analysis of the wood mixture supplied to the ASPEN/SP program[39] was carbon, 49.5 wt %; hydrogen, 6.0 wt %; oxygen, 42.7 wt %; nitrogen, 0.2 wt %; sulfur, 0.1 wt %; and ash, 1.5 wt %. This composition is representative of a hardwood mixture. Complete conversion of sawdust to gas and ash at chemical equilibrium was assumed at a pressure of 14.7 psia.

Predicted CO yields increased dramatically with increasing temperature from 538 to 871 °C (Figure 2). Above 871 °C, the CO yield remained almost constant. Much lower yields of hydrogen and methane (<10%) are predicted at the lowest temperature examined, and the predicted H_2 yield increased and the CH_4 yield decreased with an increase in the temperature, at temperatures below 982 °C. Above 982 °C, the H_2 and CH_4 yields remained almost constant at fairly low percent values (somewhat masked by the scale used in Figure 2). Predicted yields of both H_2O and CO_2 decreased when the temperature increased, essentially disappearing at temperatures above 982 °C. Reactions of interest are[31,40−42]

$$3H_2\,(g) + CO\,(g) \leftrightarrow CH_4\,(g) + H_2O\,(g) \qquad \Delta H^0_{298} = -206\ \text{MJ/kmol} \quad (1)$$

$$4H_2\,(g) + CO_2\,(g) \leftrightarrow CH_4\,(g) + 2H_2O\,(g) \qquad \Delta H^0_{298} = -165\ \text{MJ/kmol} \quad (2)$$

$$H_2O\,(g) + CO\,(g) \leftrightarrow CO_2\,(g) + H_2\,(g) \qquad \Delta H^0_{298} = -41\ \text{MJ/kmol} \quad (3)$$

$$C\,(s) + 2H_2\,(g) \leftrightarrow CH_4\,(g) \quad \Delta H^0_{298} = -75\ \text{MJ/kmol} \quad (4)$$

$$C\,(s) + CO_2\,(g) \leftrightarrow 2CO\,(g) \quad \Delta H^0_{298} = +168\ \text{MJ/kmol} \quad (5)$$

$$C\,(s) + H_2O\,(g) \leftrightarrow CO\,(g) + H_2(g) \qquad \Delta H^0_{298} = +175\ \text{MJ/kmol} \quad (6)$$

The endothermic reactions (eqs 1−4) are favored at high temperatures, while the reverse is true for exothermic reactions (eqs 5 and 6). Higher H_2 and CO yields and lower CH_4 and H_2O yields are predicted at higher temperatures.

Predicted CO and H_2 yields decreased as the pressure increased, while CO_2, CH_4, and water yields increased with the pressure (Figure 3). Pressure has little influence on the H_2 yield at higher pressures (>5 atm). Low pressures in the pyrolysis process will favor CO production. Reactions 1−3 are shifted toward the products, and the reactions 5 and 6 are shifted

(39) Green, D. *Perry's Chemical Engineers' Handbook*, 6th ed.; McGraw-Hill: NewYork, 1984.

(40) Encinar, J. M.; Beltran, F. J.; Ramiro, A.; Gonzalez, J. F. Pyrolysis/gasification of agricultural residues by carbon dioxide in the presence of different additives: Influence of variables. *Fuel Process. Technol.* **1998**, *55*, 219−233.

(41) McKendry, P. Energy production from biomass (part 3): Gasification technologies. *Bioresour. Technol.* **2002**, *83*, 55−63.

(42) Schuster, G.; Loffler, G.; Weigl, K.; Hofbauer, H. Biomass steam gasification−An extensive parametric modeling study. *Bioresour. Technol.* **2001**, *77*, 71−79.

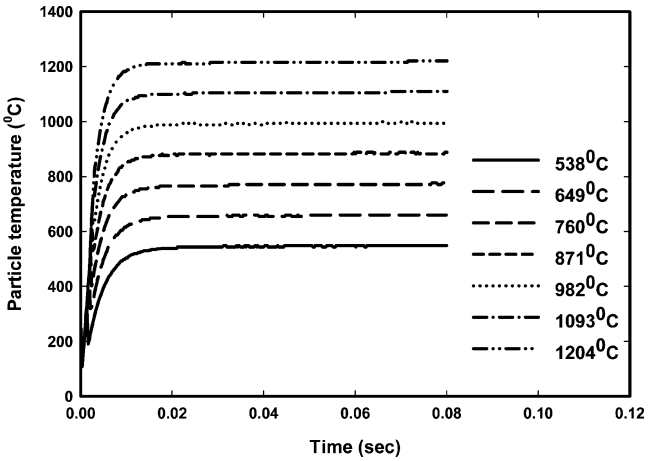

Figure 4. Time dependence of the wood particle temperature computed for various gas temperatures according to eq 13 assuming no relative gas versus particle motion (particle size = 100 μm).

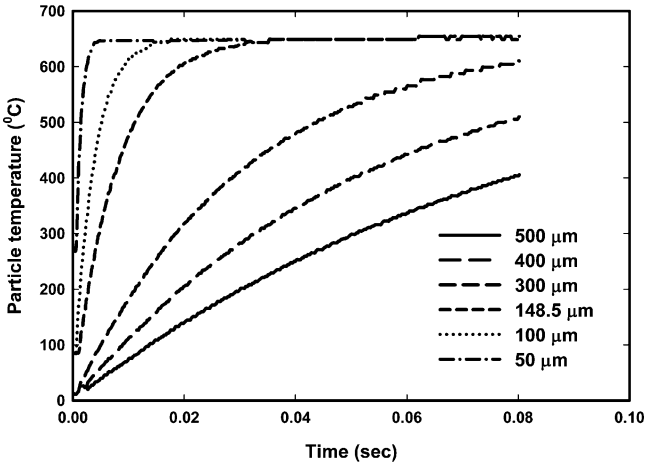

Figure 5. Time dependence of the wood particle temperature at a gas temperature of 649 °C for various particle diameters (in micrometers) computed by eq 13 assuming no relative gas versus particle motion.

toward the reactants with increasing pressure. Thus, as the pressure is increased, more CH_4 and H_2O and less CO and H_2 will form.

Predictions of the effect of the steam/carbon mole ratio on H_2, CO, CO_2, and CH_4 production were examined (data omitted for brevity). The H_2 yields at low temperature (538−954 °C, Figure 4) and at high temperature (1038−1371 °C, Figure 5), respectively, were predicted. At $H_2O/C > 1.4$, the H_2 production reached a maximum at a temperature of 704 °C. CO increased with the temperature and reached a maximum at a H_2O/C mole ratio of 0.35, above 704 °C. High CO_2 yields were obtained at high steam/carbon ratios and low temperatures. Less CH_4 was predicted at higher steam/carbon ratios and high temperatures. Very high steam/carbon mole ratios shifted reactions 1 and 2 toward the reactants. The water−gas shift (reaction 3) was shifted toward CO_2 production, resulting in lower CO and CH_4 yields and higher H_2 and CO_2 yields.

ASPEN/SP and STANJAN simulations were compared. Katofsky[43] simulated an adiabatic operation using STANJAN and assumed 100% carbon conversion to gaseous species. Species present at equilibrium were H_2, CO, CO_2, CH_4, H_2O, and N_2 (Table 1). Both ASPEN/SP and STANJAN simulations

Table 1. Chemical Equilibrium Results from ASPEN/SP versus STANJAN

overall C/H/O ratio	1/1.93/1.59	
temperature (°C)	1085	
	gas composition (mol %)	
components	ASPEN/SP	STANJAN[43]
H_2	30.48	30.67
CO	39.45	39.04
CO_2	11.41	11.77
CH_4	0.001	0.10
H_2O	18.60	18.36
N_2	0.054	0.05

gave similar results. At temperatures below 1085 °C, CO, CO_2, and H_2 were dominant, while CH_4 was only present in trace amounts.

3.2. Heat Transfer into Wood Particles. Biomass pyrolysis is extremely temperature-sensitive. The temperature profile within the biomass particle during pyrolysis is critical. If a significant temperature gradient exists within the particle or if the time required for the center of a particle to reach the reactor temperature is comparable to the time needed for the various pyrolysis reactions to occur, the lag in heat transfer must be considered. In such a case, the overall process may not be controlled by the chemical reaction kinetics.

The surface temperature of the solid is not determined solely by the reactor or carrier gas temperature. The energy generated or consumed (exo- or endothermic) during the primary and secondary pyrolysis reactions will also influence the temperature. The energy is transferred mainly by convection to volatile products at the particle surface. In addition, the velocity profile of the gas passing by the particle and direct solid/reactor wall contact will affect the temperature distribution within the solid feed.[44] This heat-transfer process is very complex. Thus, a simplified case is considered: sawdust particles suspended in the hot gas are heated by conduction from the hot gas. Radiation was assumed not to be significant at lower pyrolysis temperatures, and the particle had a unique surface temperature. The net rate of energy transfer to the particle is

$$q = hA_p(T_g - T_p) \tag{7}$$

where h is the heat-transfer coefficient corresponding to the total surface area of the hot gas particle, T_g and T_p are the gas and particle temperatures, and A_p is the surface area for the particle, respectively. The net rate of energy transfer is expressed as

$$q = m_p C_p \frac{dT_p}{dt} = \rho_p V_p C_p \frac{dT_p}{dt} \tag{8}$$

where m_p, ρ_p, C_p, and V_p are the weight, density, heat capacity, and volume of the particle, respectively. Combining eqs 7 and 8 yields

$$\rho_p V_p C_p \frac{dT_p}{dt} = hA_p(T_g - T_p) \tag{9}$$

Equation 9 can also be expressed as

$$\frac{dT_p}{dt} = \frac{6\mathrm{Nu}k_g}{\rho_p C_p d_p^2}(T_g - T_p) \tag{10}$$

(43) Katofsky, R. E. The production of fluid fuels from biomass. Princeton University, Princeton, NJ, 1993.

(44) Bilbao, R.; Murillo, M. B.; Millera, A.; Arauzo, J.; Celeya, J. M. Thermal decomposition of a wood particle. Temperature profiles on the solid surface. *Thermochem. Acta* **1992**, *197*, 431−442.

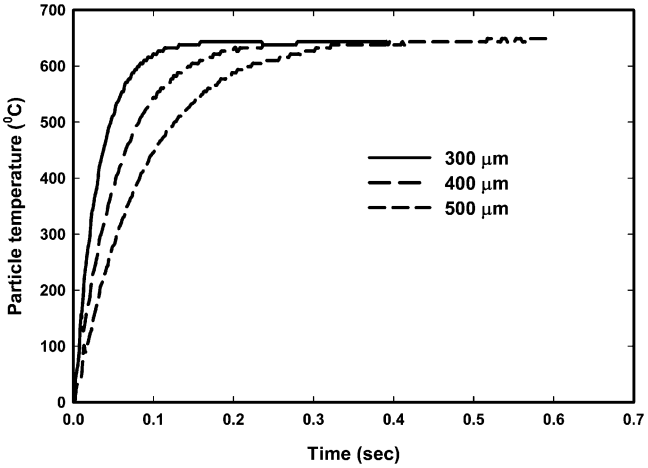

Figure 6. Time dependence of the wood particle temperature computed by eq 13 for various particle diameters (in micrometers) at a gas temperature of 649 °C assuming no relative gas versus particle motion.

where Nu is the Nusselt number, defined by eq 11

$$\mathrm{Nu} = \frac{hd_\rho}{k_\mathrm{g}} \tag{11}$$

Here, k_g is the thermal conductivity of the surrounding gas. When forced convection around submerged objects occurs, the Nusselt number is

$$\mathrm{Nu} = 2 + 0.60(\mathrm{Re})^{1/2}(\mathrm{Pr})^{1/3} \tag{12}$$

where Re is the gas fluid Reynolds number ($D_\mathrm{p}\upsilon_\mathrm{g}\rho_\mathrm{g}/\mu_\mathrm{g}$) and Pr is the fluid Prandtl number.[45] If there is no relative motion between the gas and the particle, the Nusselt number is 2. Integrating eq 10 yields eq 13[46]

$$\frac{T_\mathrm{g} - T_\mathrm{p}}{(T_\mathrm{g} - T_\mathrm{p})_0} = \exp\left(\frac{-6\mathrm{Nu}k_\mathrm{g}t}{\rho_\mathrm{p}C_\mathrm{p}{d_\mathrm{p}}^2}\right) \tag{13}$$

The particle temperature increase versus time at various gas temperatures is shown in Figure 4. The time dependence of the particle temperature in a 649 °C gas medium, computed for different particle sizes (eq 13), is shown in Figures 5 and 6. The physical constants for pine sawdust used in the calculations were $\rho_\mathrm{p} = 551.036$ kg/m^3 and $C_\mathrm{p} = 0.32$ kcal (kg °C)$^{-1}$,[39] and the thermal conductivity of nitrogen is[39]

$$k_\mathrm{g} = -9.2093 \times 10^{-3} + 8.5836 \times 10^{-5}\,\mathrm{Tg} - 1.8941 \times 10^{-8}\,\mathrm{Tg}^2\ \mathrm{W\ (m\ K)^{-1}} \tag{14}$$

Particles (100 μm) take approximately 0.026 s to reach the surrounding gas temperature at 649 °C. The time to reach the gas temperature is sensitive to the particle size as illustrated in Figures 5 and 6. Particles more than 500 μm in diameter require more than 0.48 s to reach the gas temperature. These calculations will overestimate the time required because it is assumed that the particle is not moving with respect to the gas in eq 13 with the use of Nu = 2. Thus, Figures 5 and 6 represent the slowest (longest) heating times possible in the experimental work.

3.3. Experimental Pyrolysis of Various Biomass Feeds. Experiments determined the time required to complete sawdust pyrolysis under various operating conditions. Sawdust was weighed, placed in the reactor, pyrolyzed, and reweighed after completion of the reaction. The residue ratio is defined as the mass of residue/mass of sawdust. The reaction time is defined as the time for the pyrolysis residue (char) to reach a constant mass. Experimental reaction times dropped with an increase in the reaction temperature (Figure 7). All of the three wood feeds have similar reaction times at 649 °C (Figure 8).

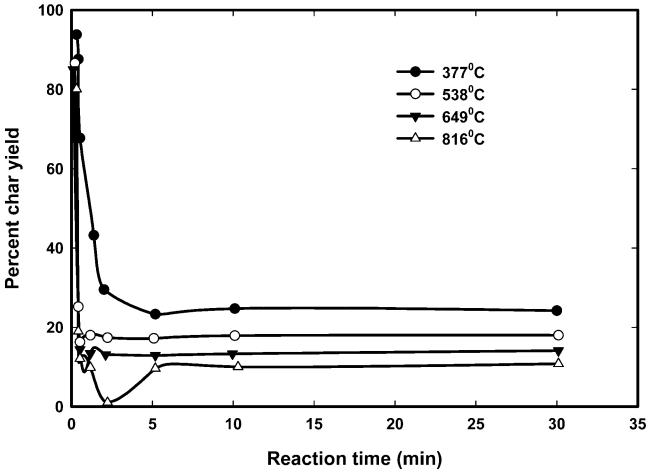

Figure 7. Effect of the reaction time on the experimental char yield during pine sawdust pyrolysis at different gas temperatures (reaction times at 816 °C).

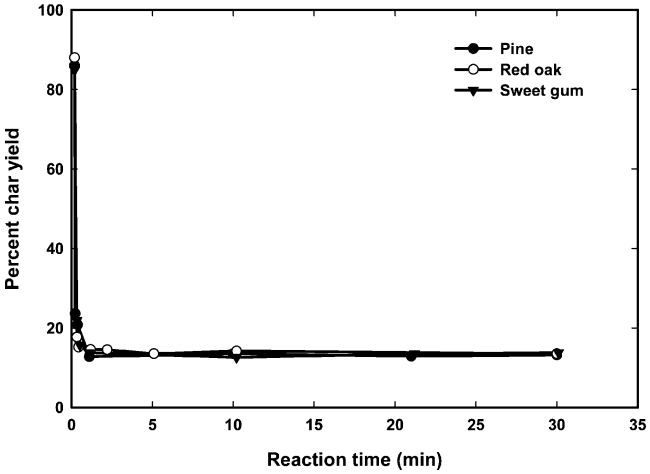

Figure 8. Effect of the reaction time on the char yield during the pyrolysis of pine, sweet gum, and red oak sawdust at 649 °C.

The pyrolysis products obtained from pine, sweet gum, and red oak at 371−816 °C were similar under identical conditions. The liquid products are summarized in Table 2, and the gaseous products are listed in Table 3. A total of 109 compounds were identified in the liquid portion, while 40 compounds were identified in the gas portion. The general similarities in the product distributions from pine, sweet gum, and red oak species at the same temperatures should not be surprising. The overall lignin, cellulose, and hemicellulose contents of these species are comparable. Softwoods, such as pine, contain lignin made of guaiacyl units, while hardwoods, such as oak, have both guaiacyl and syringyl lignin building blocks. Despite such differences, we have repeatedly found that pine and oak wood pyrolyses do not lead to large composition differences from these building blocks. For example, in an auger-fed fast pyrolysis reactor operating at 450 °C, we have observed that guaiacyl units constituted 17.3% of all carbons in the lignin-rich ethyl acetate fraction of pine bio-oil and 15.3% for oak by ^{13}C nuclear

(45) Bird, R. B.; Stewart, W. E.; Lightfoot, E. N. *Transport Phenomena*; John Wiley and Sons: NewYork, 1960.

(46) Ozturk, Z. Pyrolysis of cellulose using a single pulse shock tube. Kansas State University, Manhattan, KS, 1991.

Table 2. Liquid Products Found in Pine Wood, Red Oak, and Sweet Gum Sawdust Pyrolysis[a]

components	retention time (min)	temperature (°C)						
					649			
		377	427	538	pine	red oak	sweet gum	816
2-butanal	7.89	D	D					
1-hydroxy-2-propanone	8.04	D	D	D				
benzene	8.64			D	D	D	D	D
1-propanol	9.15	D						
1-(1-methylethoxy)-2-propanone	11.67		D					
1-hydroxy-2-propanone	12.23	D	D					
toluene	12.58			D	D	D	D	D
2-cyclopenten-1-one	14.27	D	D	D	D			
2-furancarbox-aldehyde	14.4	D	D	D				
2-butanone	14.83	D	D	D				
2-furanmethanol	15.49	D	D	D				
ethylbenzene	16.37			D	D	D	D	
2(5*H*)-furanone	16.67	D	D					
1,3-dimethyl-benzene	16.71			D	D	D	D	
phenylethyne	16.74							D
2-cyclohexen-1-ol	17.01	D	D	D				
styrene	17.39			D	D	D	D	D
p-xylene	17.59			D	D	D	D	
cyclohexanone	17.87	D		D				
2-cyclohexen-1-one	18.27	D	D	D				
3,3-dimethyl-2-butanone	19.13	D						
3-methyl-2-cyclopenten-1-one	19.37			D	D		D	
hydroquinone	19.44	D	D					
phenol	20.21	D	D	D	D	D	D	D
2,5-piperazinedione	20.48	D	D					
α-methylstyrene	20.83					D	D	
1,4-cyclohexanedione		D						
benzofuran	21.28			D	D	D	D	D
2,3-dihydro-3-methylfuran	21.05	D	D					
3-methyl-1,2-cyclopentanedione	21.86	D	D					
1,4-diethoxy-2-butene	21.94	D						
2-ethyl-1,3-dioxolane	22.38	D	D	D				
2-methylphenol	22.83	D	D		D	D	D	
indene	23.05			D	D	D	D	D
4-methylphenol	23.48	D	D	D	D	D	D	
2-propanamine	23.94	D	D					
butanal	24.48	D						
7-methylbenzofuran	24.99			D	D	D	D	
3-phenyl-2-propenal	25.11			D	D	D		
2-methoxyphenol	25.16	D	D					
2-ethylphenol	25.59				D	D	D	
cyclobutanone	25.79	D						
2,4-dimethylphenol	25.96				D	D	D	
5-methyl-2-heptanamine	25.16	D						
2-ethylphenol	26.46				D		D	
3-ethyl-2-hydroxy-2-cyclopenten-1-one	26.47		D					
1-methyl-1*H*-indene	26.75			D	D	D	D	
4-(methylthio)acetophenone	26.75		D					
3,5-dimethylphenol	27.32	D	D	D	D	D	D	
cyclopentanol	27.63	D						
naphthalene	27.64			D	D	D	D	D
2,3-dihydrobenzofuran	27.88	D			D	D	D	
1,2-benzenediol	28.29	D	D	D	D		D	
cis-1,2-cyclohexanediol	28.65		D					
4-ethylphenol	28.77		D	D				
3(2*H*)-benzofuranone	28.88				D			
2,3-dihydro-1*H*-indene-1-one	29.94				D		D	
1,4:3,6-dianhydro-α-D-glucopyranose	30.03		D					
2-(2-propenyl)phenol	30.14				D		D	
2-methoxy-4-methylphenol	30.17	D	D					
5-(hydroxymethyl)-2-furancarboxaldehyde	30.34	D	D					
2,3-dihydrobenzofuran	30.79		D	D		D		
2-methylnaphthalene	30.99				D	D	D	D
3-phenyl-2-propenal	31.38				D		D	
1-methylnaphthalene	31.46				D	D	D	D
2-(1-methylethyl)phenol	31.90		D	D				
ethenylbenzaldehyde	32.01				D		D	
hydroquinone	32.37	D						
3-methyl-1,2-benzenediol	32.45	D	D	D				
biphenyl	33.18				D	D	D	D
4-methyl-1,2-benzenediol	33.52	D	D	D				
4-ethyl-2-methoxyphenol	33.61	D						

Table 2. Continued

components	retention time (min)	temperature (°C) 377	427	538	649 pine	649 red oak	649 sweet gum	816
2-ethylnaphthalene	33.74				D	D	D	
2-(2-propenyl)phenol	33.75		D	D				
1,8-dimethylnaphthalene	34.05				D	D		
1,7-dimethylnaphthalene	34.45				D	D		
2,6-dimethylnaphthalene	34.55				D	D		
2-ethenylnaphthalene	36.64							D
1-(3-methoxy-phenyl)ethanone	34.74	D						
acenaphthylene	35.19				D	D	D	D
1,4-dimethylnaphthalene	35.37				D	D	D	
4-(2-propenyl)phenol	35.42	D	D					
2-methyl-1,1′-biphenyl	35.94				D			
1-naphthalenol	36.11				D	D	D	
eugenol	36.27	D						
2-naphthalenol	36.3				D	D	D	
4-ethyl-1,3-benzenediol	36.73	D	D					
dibenzofuran	36.92				D	D	D	D
vanillin	37.06	D	D					
3-methyl-1,1′-biphenyl	37.52				D	D	D	
1,6-anhydro-β-D-glucopyranose	37.77	D	D	D				
2-methoxy-4-(1-propenyl)phenol	37.90	D						
fluorene	38.55				D	D	D	D
2-methyl-1-(1,1-dimethylethyl)-2-methyl-1,3-propanediylpropanoate	38.71				D	D	D	D
2′,4′-dihydroxypropiophenone	39.04	D						
2-methoxy-4-(1-propenyl)phenol	39.31	D	D					
9*H*-fluorene-9-carboxylic acid	39.56				D	D	D	
1-(4-hydroxy-3-methoxy-phenyl)ethanone	40.16	D	D					
1-methyl-9-*H*-fluorene	41.26				D			
4-methyl-9-*H*-fluorene	41.41				D			
4-ethyl-2-methoxyphenol	41.85	D						
phenanthrene	43.05				D	D	D	D
anthracene	43.32				D	D	D	D
3,5-dimethylbenzoic acid	44.99		D					
4-hydroxy-3-methoxybenzeneacetic acid	46.43	D						
2-phenylnaphthalene	46.87							D
fluoranthene	48.81					D		D
3-methoxycinnamic acid	48.96	D						
pyrene	49.83							D

[a] D = detectable.

magnetic resonance (NMR) spectroscopy.[47] Syringyl-derived units made 2.7% of this fraction for pine and 7.4% for oak. Some syringyl units may be thermally converted to guaiacyl derivatives during pyrolysis.

At 538 °C, the major liquid components were ketones, alcohols, cresols, and smaller amounts of aromatic compounds (Table 2). Above 538 °C, benzene, phenols, cresols, and other aromatic compounds dominated. The polycyclic aromatic compounds, pyrene, fluoranthene, phenanthrene, anthracene, naphthalene and acenaphthalene, were detected above 760 °C, and their yields increased with increasing temperature.

Wood pyrolysis proceeds via primary and secondary reactions. Cellulosic ring fragmentations, depolymerizations, and dehydrations are primary reactions that form carbonyls, carboxylic acids, and alcohols, while anhydrosugars (primarily levoglucosan) are obtained from depolymerization and water loss. Dehydration reactions produce char, water, gas, and tar.[48] Levoglucosan was detected in the liquid product generated below 649 °C. Secondary reactions became more important at higher temperatures and residence times. Decarboxylation and dehydration reactions favor the production of olefins. Propylene, ethylene, and butane were produced at higher temperatures. Olefin production is followed by reactions to form cyclic olefins. The six-carbon ring intermediates then undergo dehydrogenation to benzene and its derivatives. Associative reactions lead to the formation of polycyclic aromatic hydrocarbons at even higher temperatures.[49]

Table 4 provides a compilation of the yields for gaseous products from pine sawdust at various pyrolysis temperatures. The yield of a component is defined as the mass of the component (calculated from quantitative analytical results) divided by the original pyrolysis sample mass. Table 5 provides quantitative results for the liquid product from pine sawdust at various pyrolysis temperatures.

3.3.1. Influence of the Temperature. Products from pyrolysis carried out at 538−816 °C were quantitatively analyzed. The gaseous products, namely, hydrogen, carbon monoxide, methane, ethylene, ethane, propylene, and methanol were the predominant species. Table 6 shows the temperature at which the maximum yield for each of these species was obtained. The experimental temperature dependence of specific gas products is shown in Figures 17−20. Yields of hydrogen, carbon monoxide, carbon dioxide, and methane increased with increas-

(47) Ingram, L.; Mohan, D.; Bricka, M.; Steele, P.; Strobel, D.; Crocker, D.; Mitchell, B.; Mohammad, J.; Pittman, C. U. J. Pyrolysis of wood and bark in an auger reactor: Physical properties and chemical analysis. **2007**, manuscript in preparation.

(48) Graham, R. G. A characterization of the fast pyrolysis of cellulose and wood biomass. University of Western Ontario, London, Ontario, Canada, 1993.

(49) Williams, P. T.; Horne, P. A. The influence of catalyst regeneration on the composition of zeolite-upgraded biomass pyrolysis oils. *Fuel* **1995**, *74*, 1839−1851.

Table 3. Gas Products from Sawdust Pyrolysis[a]

components	retention time (min)	temperature (°C) 377	427	538	649	816
hydrogen	1.01	D	D	D	D	D
carbon monoxide	1.68	D	D	D	D	D
methane	2.09	D	D	D	D	D
carbon dioxide	2.90	D	D	D	D	D
ethylene	4.20		D	D	D	D
acetylene	4.22			D	D	D
ethane	5.31		D	D	D	D
propylene	11.86		D	D	D	D
propane	12.49		D	D	D	D
1,2-propadiene	13.05			D	D	D
methanol	14.13	D	D	D	D	D
acetaldehyde	15.61	D	D	D	D	D
methyl formate	17.56	D		D		D
2-methyl-1-propene	17.95			D	D	
1-butene	18.05	D		D	D	
1,3-butadiene	18.18	D		D	D	
2-methyl-1-propene	18.65			D	D	
1,2-butadiene	19.26			D		D
2-propenal	20.69	D	D	D	D	
furan	20.89	D	D	D	D	
propanal	21.26	D	D	D	D	
acetone	21.51	D	D	D	D	
1,1-dimethylcyclopropane	22.09				D	
(*Z*)-1,3-pentadiene	22.35				D	
methyl acetate	22.68	D		D	D	D
3-penten-1-yne	23.10			D	D	D
1,3-cyclopentadiene	23.11				D	
2-methyl-1,3-butadiene	23.27			D	D	
2-methyl-1-butene	23.47			D		
1,1-dimethyl-cyclopropane	23.55			D		
2,3-pentadiene	24.12			D		
2,5-dihydrofuran	24.61	D	D	D		
2-methylpropanal	24.71			D		
3-buten-2-one	25.35	D	D	D		
2-methylfuran	25.57	D	D	D	D	
2,3-butanedione	25.65	D	D	D		
2-butanone	25.84	D	D	D	D	
2-hexene	27.17			D		
2-butenal	27.22	D	D	D		
3,3-dimethycyclobutene	27.67			D		

[a] D = detectable.

ing temperature, while yields of methanol, acetaldehyde, acetone, and propanal decreased. Secondary dehydrations and ethane cracking can account for the increase in hydrogen with increasing temperature. CO is the most abundant secondary product, reaching a maximum yield of ~46% at 871 °C (Figure 9). CO forms in secondary reactions when primary vapors are cracked to low-molecular-weight, noncondensable gases. Methane formation increased with the temperature, reaching a maximum yield of 8% at 760 °C (Figure 9). Methane, produced from both the primary and secondary reactions, is very stable, but at extremely high temperatures, methane can react with oxygen to form acetylene. This is evidenced by an increased yield of acetylene at temperatures above 760 °C (Figure 10).

Ethane production decreased because of cracking above 593 °C. Ethane cracking produces mostly ethylene and hydrogen as well as smaller amounts of methane and traces of benzene, propylene, and naphthalene.[48] Thus, both ethylene and hydrogen yields increased above 593 °C. The yield of CO_2 increased only slightly between 371 and 816 °C. Scott et al.[49] observed a plateau in the CO_2 yield from 371 to 427 °C[50] because it is a primary product in the initial cellulose and hemicellulose decomposition pathway, which reached a limiting yield at ~371 °C. As secondary decompositions become more significant at higher temperatures, the CO_2 yield increases. However, the residence times used in this work may allow the water−gas shift reaction to consume more CO_2 than that observed by Scott and co-workers.[50] Cracking of propylene, 1,2-butadiene, and other butane isomers under high temperatures may be responsible for the decrease in their yields. Decarboxylations and dehydrations increase with the temperature, causing a drop and disappearance of methanol, acetaldehyde, propanal, and acetone (Figures 11 and 12).

Selected liquid component yields are depicted in Figures 13 and 14. The temperatures at which the maximum yield was obtained for each species shown in Figures 13 and 14 are given in Table 7. Higher yields of benzene and naphthalene were found at higher temperatures, but they were not detected below 538 °C (Figure 13). A similar trend was found for toluene, cresol, dimethyl phenol, and phenol. Maximum yields of these compounds were obtained between 650 and 704 °C. Polycyclic

Table 4. Percent Yields of Gaseous Products from Pine Sawdust Pyrolysis at Different Temperatures[a]

components	percent yield 538 °C	593 °C	649 °C	704 °C	760 °C	816 °C
hydrogen	0.20	0.35	0.55	0.71	0.92	1.18
carbon monoxide	14.40	24.70	31.73	35.14	36.85	40.68
methane	2.06	3.18	5.45	6.62	6.89	7.53
carbon dioxide	8.34	8.74	9.22	9.72	9.81	10.05
ethylene	0.83	1.79	1.83	3.36	3.66	3.51
acetylene	BDL	BDL	BDL	BDL	0.24	0.32
ethane	0.40	0.78	0.59	0.61	0.38	0.17
propylene	0.60	1.16	0.79	0.55	0.23	0.11
propane	0.08	0.11	0.06	0.04	trace	trace
1-propyne	0.002	0.01	0.01	0.01	0.01	trace
1,2-propadiene	0.26	0.04	0.03	0.03	0.02	0.16
acetaldehyde	3.27	2.13	1.42	0.33	0.05	trace
methanol	1.26	0.99	1.00	0.66	0.31	0.11
1-butene	0.19	0.24	0.13	0.04	BDL	BDL
1,2-butadiene	0.09	0.20	0.22	0.22	0.13	0.08
2-butene	0.06	0.09	0.04	0.01	BDL	BDL
2-methyl-1-propene	0.03	0.06	0.038	0.01	BDL	BDL
propanal	0.32	0.21	0.09	0.01	BDL	BDL
acetone	0.23	0.22	0.20	0.06	BDL	BDL
2-methyl-1-buten-3-yne	0.18	0.36	0.19	0.26	0.16	0.28
2-butenal	0.19	0.10	trace	BDL	BDL	BDL
3-buten-2-one	0.22	0.14	BDL	BDL	BDL	BDL
acetic acid ethyl ester	0.12	BDL	BDL	BDL	BDL	BDL
2-methylpropanal	0.09	0.07	BDL	BDL	BDL	BDL
sum of gas products	34.74	49.31	49.94	60.48	61.86	65.29

[a] BDL = below detection limit.

Table 5. Percent Yields of Liquid Products and Char from Pine Sawdust Pyrolysis at Different Temperatures[a]

components	percent yield					
	538 °C	593 °C	649 °C	704 °C	760 °C	816 °C
benzene	0.05	0.44	0.66	1.32	1.43	1.80
toluene	0.12	0.31	0.58	0.48	0.51	0.34
ethylbenzene	trace	0.04	0.06	BDL	BDL	BDL
m- and *p*-xylene	trace	0.11	0.18	0.16	0.09	0.03
styrene	trace	0.11	0.28	0.40	0.31	0.28
o-xylene	0.03	0.04	0.07	0.05	0.02	BDL
ethylmethylbenzene	BDL	trace	0.12	trace	BDL	BDL
cyclopropyl benzene	BDL	BDL	0.04	0.01	BDL	BDL
phenol	0.18	0.32	0.63	0.80	0.32	0.23
OC-methylstyrene	BDL	BDL	0.03	trace	BDL	BDL
2-methylphenol	0.13	0.25	0.30	0.11	0.03	trace
4-methylphenol	0.18	0.37	0.34	0.21	0.07	trace
indene	BDL	0.07	0.16	0.44	0.31	0.31
2,3-dimethylphenol	BDL	0.02	0.03	0.02	BDL	BDL
2-ethylphenol	BDL	0.02	0.02	BDL	BDL	BDL
2,4-dimethylphenol	0.12	0.11	0.13	0.01	BDL	BDL
2,6-dimethylphenol	0.02	0.03	0.04	trace	BDL	BDL
4-ethylphenol	0.05	0.09	0.04	0.01	BDL	BDL
1,2-benzenediol	0.23	0.13	trace	BDL	BDL	BDL
naphthalene	BDL	0.05	0.18	0.49	0.53	0.90
3-(1-methylethyl)phenol	0.01	trace	BDL	BDL	BDL	BDL
2-ethyl-5-methylphenol	0.04	0.03	trace	BDL	BDL	BDL
4-methyl-1,2-benzenediol	0.04	0.01	BDL	BDL	BDL	BDL
3-methyl-1,2-benzenediol	0.17	0.04	BDL	BDL	BDL	BDL
2-(2-propenyl)phenol	0.05	0.05	trace	BDL	BDL	BDL
1-methylnaphthalene	BDL	0.03	0.07	0.14	0.08	0.07
2-methylnaphthalene	BDL	0.02	0.06	0.08	0.05	0.04
biphenyl	BDL	BDL	trace	0.03	0.04	0.04
1,3-dimethylnaphthalene	BDL	BDL	0.01	trace	BDL	BDL
acenaphthalene	BDL	trace	0.04	0.14	0.15	0.22
fluorene	BDL	trace	0.01	0.05	0.06	0.09
anthracene	BDL	BDL	trace	0.08	0.11	0.17
phenathrene	BDL	trace	0.03	0.03	0.04	0.06
fluoranthene	BDL	BDL	trace	0.02	0.05	0.09
pyrene	BDL	BDL	trace	0.02	0.05	0.09
sum of C6−C16	1.45	2.67	4.11	5.13	4.25	4.76
char	17.42	14.70	14.04	12.56	11.29	10.64
sum of gases	34.74	49.31	49.94	60.48	61.86	65.29
total mass yield	53.61	66.68	68.09	78.17	77.39	80.70

[a] BDL = below detection limit.

Table 6. Experimental Optimum Pyrolysis Temperature That Generates the Maximum Yields of Major Gas-Phase Compounds

compounds	reactor temperature (°C)	yield percent weight of sawdust
hydrogen	816	1.18
carbon monoxide	816	40.68
methane	816	7.53
carbon dioxide	816	10.05
ethylene	816	3.51
ethane	593	0.78
acetylene	816	0.32
propylene	593	1.16
propane	593	0.11
acetaldehyde	538	3.26
methanol	538	1.26
1,2-butadiene	649	0.22
butenes (sum of 1-butene and 2-butenes)	593	0.24
propanal	538	0.32
acetone	538	0.23

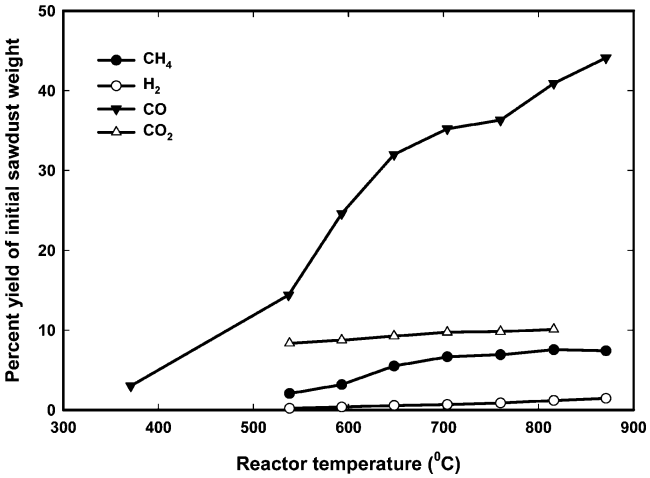

Figure 9. Effect of the reaction temperature on the yield of CH_4, H_2, CO, and CO_2 during the pyrolysis of pine sawdust.

aromatic products became dominant as the temperature approached 704 °C, while toluene, cresol, and dimethyl phenol began to disappear. Toluene cracks at these temperatures. Below 704 °C, acids and alcohols derived from nonrandom fragmentation of cellulose, hemicellulose, and lignin undergo subsequent dehydration, decarboxylation, and recombination reactions, forming toluene, cresol, dimethyl phenol, and phenol. At very high temperatures, these components undergo continued dehydration and decarboxylation, raising the benzene yield. Associative oligomerizations lead to the subsequent formation of polycyclic aromatic hydrocarbons, such as pyrene, fluoranthene, phenanthrene, anthracene, and fluorine.

3.3.2. Influence of the Sawdust Particle Size. Sawdust particles of varying diameter ($d < 105$ μm, 105 μm $< d <$ 149 μm, 149 μm $< d <$ 297 μm, and $d >$ 297 μm) were used to study the

(50) Scott, D. S.; Piskorz, J.; Bergougnou, M. A.; Graham, R.; Overend, R. P. The role of temperature in the fast pyrolysis of cellulose and wood. *Ind. Eng. Chem. Res.* **1988**, *27*, 8−15.

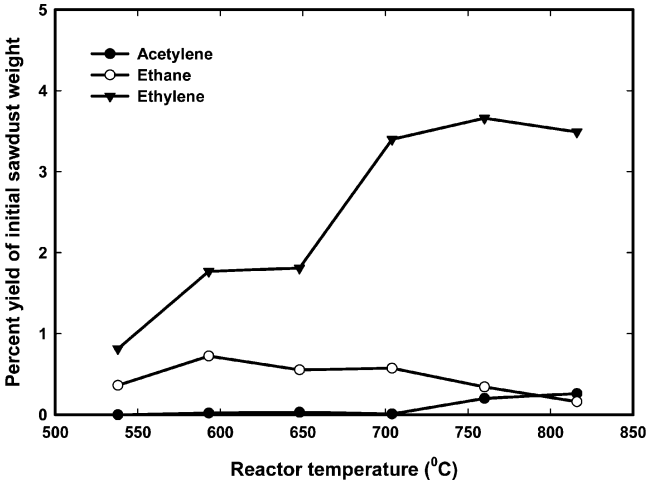

Figure 10. Effect of the pine sawdust pyrolysis temperature on C2 products.

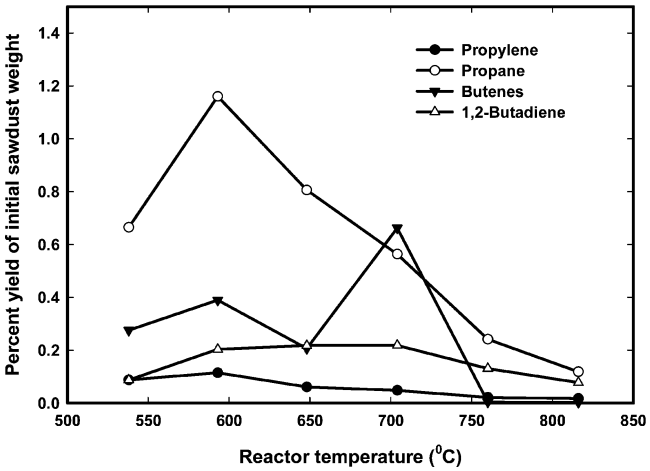

Figure 11. Effect of the pine sawdust pyrolysis temperature on C3 and C4 products.

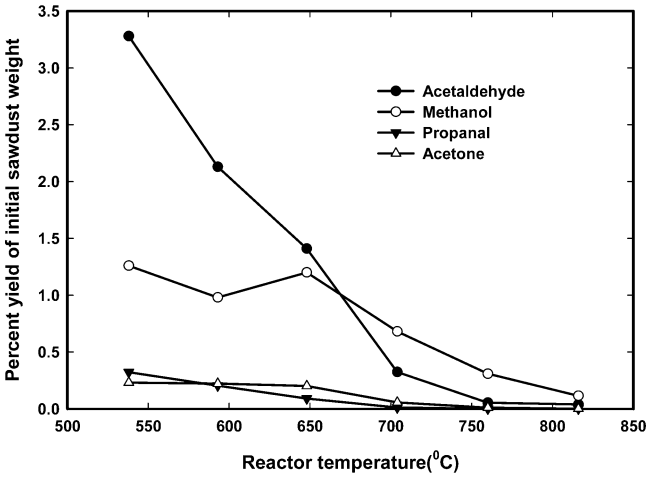

Figure 12. Effect of the pine sawdust pyrolysis temperature on methanol, acetaldehyde, acetone, and propanal yields.

effect of the particle size on pyrolysis. The yields of H_2, CO, and CH_4 versus particle size are shown in Figure 15. The centers of smaller particles more rapidly reach the reactor temperature than those of large particles. Furthermore, smaller particles have a higher surface/ volume ratio, allowing primary pyrolysis fragments to escape more rapidly into the vapor. Thus, secondary reactions are less favored.[51] Oils or tar from primary

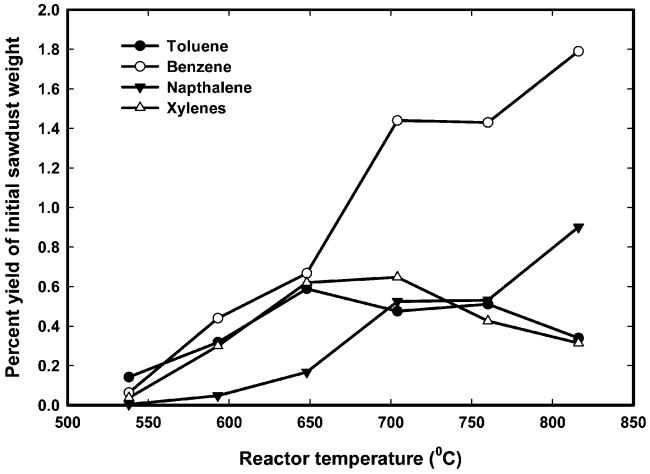

Figure 13. Effect of the pine sawdust pyrolysis temperature on benzene, toluene, xylene, and naphthalene yields.

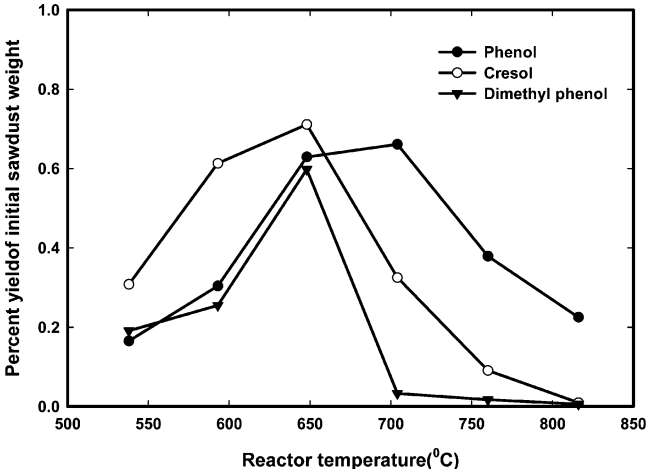

Figure 14. Effect of the pine sawdust pyrolysis temperature on phenol, cresol, and dimethyl phenol yields.

Table 7. Experimental Optimum Pyrolysis Temperature That Gives the Maximum Yields of Major Liquid Compounds

compounds	temperature (°C)	yield percent weight of sawdust
benzene	816	1.80
toluene	650	0.58
xylene	704	0.65
naphthalene	816	0.90
phenol	704	0.66
cresol	650	0.70
dimethyl phenol	650	0.60

pyrolysis further fragments into smaller molecules, producing gases, and condense to chars in secondary reactions. It is clear from Figure 15 that the particle size did not have a pronounced effect on the yield of H_2, CO, and CH_4 within the size range tested. Therefore, heat-transfer limitations did not significantly influence the range of reactions occurring for the particle size range examined. Furthermore, the escape of volatiles was fast enough in the particle size range examined; therefore, major differences in the extent of secondary reactions were not observed. For the particle size range examined through experiments, simulation results (Figure 5) indicate that the time required for the particle center to achieve the gas temperature

(51) Nunn, T. R.; Howard, J. B.; Longwell, J. P.; Peters, W. A. Product compositions and kinetics in the rapid pyrolysis of sweet gum hardwood. *Ind. Eng. Chem. Process Res. Div.* **1985**, *24*, 836−844.

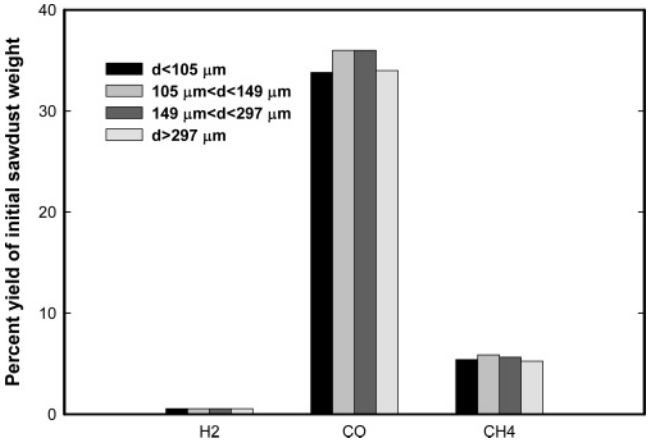

Figure 15. Effect of the particle size on H_2, CO, and CH_4 yields during pine sawdust pyrolysis.

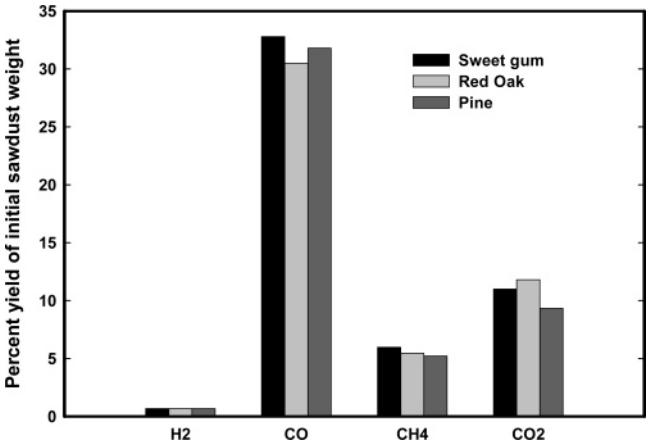

Figure 16. Yields of major gas products in pyrolysis of three different varieties of sawdust (reactor temperature = 649 °C).

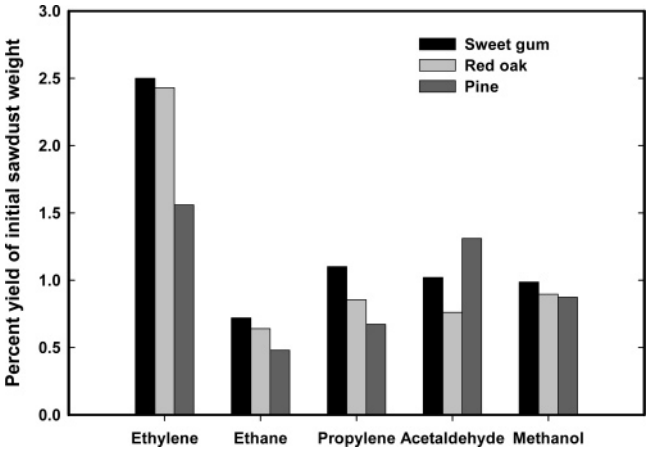

Figure 17. Yield of ethylene, ethane, propylene, acetaldehyde, and methanol gas products from pyrolysis at 649 °C of three different sawdust species.

varies only from <0.02 s (100 μm in diameter) to ~0.1 s (300 μm in diameter). Thus, the experimental findings confirm that, in the size range examined, the particle diameter does not influence the composition of the gas product.

3.3.3. Influence of the Wood Species on Products. Sweet gum, red oak, and pine sawdust samples were pyrolyzed at 649 °C (Figures 16−18). Each species produced similar gas product distributions. Pine produced the smallest yield of gaseous

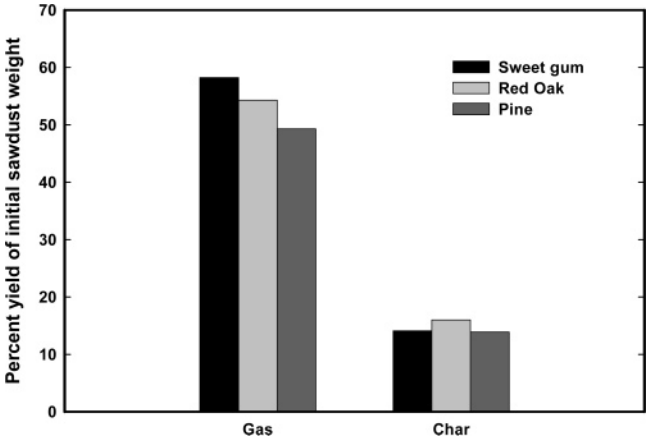

Figure 18. Gas and char yields from pyrolysis at 649 °C of three different sawdust species.

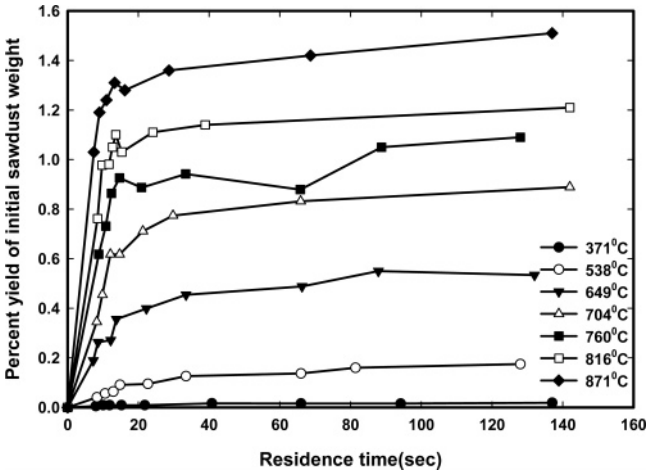

Figure 19. Effect of the gas residence time and temperature on the H_2 yield during sawdust pyrolysis.

product, and red oak gave the highest char yield. Sweet gum sawdust produced the largest yield of gas, except for CO_2 and acetaldehyde. However, the overall effect of the wood species was small.

3.3.4. Influence of the Gas Residence Time. The gas-phase residence time determines the extent to which gas-phase secondary reactions occur. Very short gas residence times enhance liquid production because secondary cracking of these primary products does not proceed as far. The influence of the residence time on the production of hydrogen, carbon monoxide, and methane was studied.

Assuming an isothermal operation of a plug-flow reactor, the gas residence time was calculated using eq 15

$$\text{residence time(s)} = (LA_c)/\nu \qquad (15)$$

where L is the effective reactor length or the length from the outlet to the position of the boat, A_c is the inner cross-sectional area of the tubular reactor, and ν is the volumetric flow rate of the purge gas. The purge gas was assumed to have the same temperature as the reactor wall when it reached the reacting sawdust. The effect of the gas residence time on H_2, CO, and CH_4 is shown in Figures 19−21. Gas production was much higher at small residence times. The rate of increase in the gas yield with increasing residence times finally reached a constant value after a specific residence time had elapsed. The residence time that gave the highest gas yield was dependent upon the

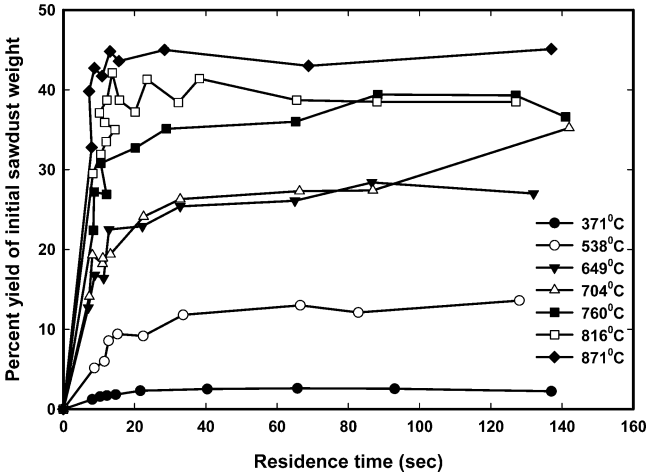

Figure 20. Effect of the gas residence time and temperature on the CO yield during pine sawdust pyrolysis.

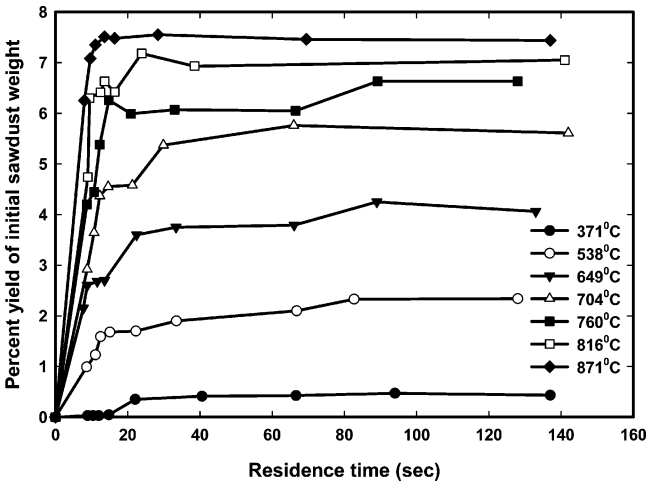

Figure 21. Effect of the gas residence time and temperature on the CH_4 yield during pine sawdust pyrolysis.

temperature. As the temperature increased, shorter residence times were required to achieve maximum yields. More gas was produced at higher reaction temperatures.

4. Conclusions

The pyrolysis of sweet gum, red oak, and pine sawdust under nitrogen or helium at 371−871 °C produced gas, liquid, and char. GC and GC/MS identified 109 liquid and 40 gas compounds. A total of 59 compounds (35 liquids and 24 gaseous products) were quantitatively determined. Gas production increased with an increasing reaction temperature, accounting for a 65 wt % conversion of the sawdust at 816 °C. Carbon monoxide was the dominant gas product (46 wt % at 871 °C). Methanol, acetaldehyde, acetone, propanol, and char yields decreased as the temperature increased. Liquid products accounted for less than 5 wt % of the raw sawdust. Benzene was the major liquid product. Its yield increased with the temperature and reached 1.8 wt % at 816 °C. Below 538 °C, the major liquid components were ketones, alcohols, and cresols; almost no hydrocarbons were present. From 538 to 760 °C, hydrocarbons, such as benzene and toluene, as well as phenols and other aromatic compounds became the major liquid products, while the amount of cresols dropped. Above 760 °C, benzene and the polycyclic aromatic compounds, such as pyrene, naphthalene, phenanthrene, and anthracene, were the major liquid products. In general, fewer oxygenates appeared in both gas and liquid products at higher temperatures.

The effects of the gas-phase residence time and sawdust particle size were also studied. Short residence times favored liquid versus gas production. Gas production at first increased dramatically with an increase in the residence time and then plateaued at a constant value. At higher reaction temperatures, the gas production increased to this plateau in shorter residence times. The particle size did not affect the pyrolysis product significantly. Thus, heat-transfer limitations within sawdust particles were not product-controlling under the operating conditions used. Pine, red oak, and sweet gum species all generated similar product distributions.

Simulations of both biomass gasification and biomass pyrolysis processes were also undertaken, using a representative composition for wood sawdust, with a limited subset of chemical reactions considered. For gasification, the influence of both the temperature and steam/carbon ratio were examined. The influence of the temperature was examined. The predicted yield of the gas product was greater for the gasification process compared to the pyrolysis process at similar reaction conditions. The predicted CO yield in pyrolysis increased with increasing temperature and reached 70% by weight at temperatures above 871 °C.

EF0606557